Review of the In-Orbit Thermal Performance of the Maritime Communication Satellite MCS-A

D.R. Chalmers*
ERNO Raumfahrttechnik GmbH, Bremen, Federal Republic of Germany

The Maritime Communication Satellite MCS-A was successfully launched in December 1981 onboard ARIANE L04, and became fully operational in May 1982. Presented in this paper are details concerning the performance of the thermal control subsystem over the initial 18 months of the mission. The relevant telemetried data was processed to allow, using the thermal mathematical models as well as direct comparison methods, an evaluation of the in-orbit thermal behavior, and thus obtain an indication of how successfully the thermal control techniques and philosophy have performed. Particular attention was focused on the technologies flying for the first time on a European satellite, i.e., the heat-pipe radiator and automatic electronic heater switching. Valuable information has been obtained for future application, not only to MCS-A, but also for the family of the European Communication Satellite, of which MCS-A was the first.

Introduction

FOLLOWING the successful launch onboard ARIANE L04 in December 1981, MCS-A became the first operational satellite from the family of European Communication Satellites (ECS) and a successor to the Orbital Test Satellite[1,2] (OTS-2) which recently celebrated its fifth successful anniversary in orbit.

The launch of MCS-A was followed (after separation from ARIANE) by a spin-stabilized period of approximately 36 h during the transfer orbit (TO). The apogee boost motor (ABM) was successfully fired at Apogee 4 bringing the satellite into a drift (near-synchronous) orbit lasting approximately 16 days. The allocated on-station position of 26°W was acquired on Jan. 5, 1982. The maritime-dedicated payload was commissioned during a three-month acceptance test phase (ATP) before MCS-A became the prime satellite for the Atlantic Ocean region of the International Maritime Satellite Organization (INMARSAT) space segment; its function is described in Fig. 1.

Spacecraft Description

Spacecraft Design

MCS-A was conceived as a three-axis stabilized vehicle based on the module or bus philosophy employed by ECS with a summary of key satellite characteristics presented in Table 1. The satellite basically consists of five main sections as shown in Fig. 2 and described briefly below.

Antennas

In all, three antennas are mounted to the upper floor—4 and 6 GHz horns and an L-band dish—the functions of which are: 1) receive signals in the 6 GHz band (C-band) for shore-to-satellite uplink, 2) transmit signals in the 1.5 GHz band (L-band) for satellite-ship downlink; 3) receive signals in the 1.6 GHz band (L-band) for the satellite-ship uplink; and transmit signals in the 4 GHz band (C-band) for the satellite-shore downlink; and transmit signals in the 4 GHz band (C-band) for the satellite-shore downlink.

Presented as Paper 83-1494 at the AIAA 18th Thermophysics Conference, Montreal, Canada, June 1-3, 1983; received Aug. 22, 1983; revision received Nov. 26, 1983.

*Senior Member Technical Staff, ERNO Thermal Control Department.

Communications System (CM)

The units and equipment comprising the communications subsystem are mounted primarily on the upper platform (low dissipating units) and dedicated north and south radiators (high dissipating units). Operation of the transponder subsystem requires that four to six of the ten available power amplifier modules (PAM's) be constantly on, and these are arranged on the north radiator. The south radiator contains the

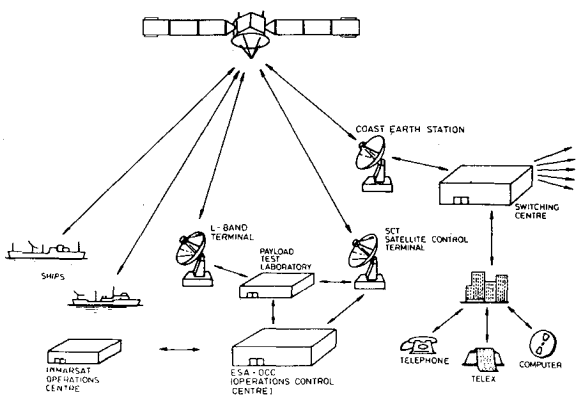

Fig. 1 Operational utilization of MCS by INMARSAT.

Table 1 MCS-A key spacecraft characteristics

Spacecraft mass	1014 kg at launch 572 kg at BOL O/S
Spacecraft dimensions	2.2 m diametrical envelope 2.9 m height 13.8 m deployed arrays
Electrical power	114 W TO (worst case) 1076 W BOL O/S (equinox) 750 W EOL (worst-case solstice)
Stabilization	Spin (60 rpm) in TO three-axis O/S
Orbital position	26°W
Stationkeeping accuracy	±0.2°E-W, ±3.0°N-S
Antenna coverage	Global to within 5 deg elevation
Design life	7 years
Launcher capability	ARIANE, STS/PAM-D

traveling wave tube amplifiers (TWTA's) and associated electronic power conditions (EPC's) as well as the transponder power supply unit (TPA-PSU).

Solar Array

Satellite power during sunlight is provided from five panels on two solar array wings (one dummy panel for symmetry), providing approximately 750 W at the end of the planned 7-y mission.

Service Module (SM)

On the lower platform (around the central tube), most of the service units and equipment from the attitude and orbit control subsystem (AOCS); telemetry, tracking, and command (TTC) subsystem; and the power subsystem (PSS), are highly dissipating units/components mounted on two dedicated north and south radiators—e.g., shunt regulator unit (SRU) and battery discharge regulators. Two 28-cell, 21-Ah Ni-Cd batteries mounted on diagonally opposite corners of the lower platform are carried in order to maintain fully satellite operation during eclipses. A hydrazine-fueled reaction control subsystem (RCS) provides for orbit and attitude maneuvers and momentum wheel loading using 16 catalytic thrusters in two redundant branches, pressurized from four bladder tanks.

Apogee Boost Motor

The ABM is installed within the satellite's central tube and is to the maximum degree thermally decoupled from the rest of the satellite.

Thermal Control Subsystem

The history associated with the formulation, design, development, and testing of a TCS for MCS-A has already been well-documented[3]; a summary of which follows.

Thermal control of MCS-A is achieved basically through conventional passive methods such as the optimizing of surface material thermo-optimal properties, controlled conductive interfaces, and selective positioning of units/components within the satellite. This is augmented by automatically and ground commanded heater circuits, whenever necessary, as well as using an integrated heat-pipe doubler on the transistor power amplifier (TPA) radiator. The selected heat pipes were of the stainless-steel, constant-conductance, artery-wick type, using ammonia as the working fluid. A total of 11 heat pipes were soldered onto a doubler (Fig. 3) which, in turn, was mounted ot the north radiator.

Within the main body of the satellite (CM and SM), the north and south panels are covered by optical solar reflectors (OSR) employed as radiators to an extent determined by the internally dissipated energy to be rejected from the satellite. The final thermal design required approximately 72% of the available radiator area to reject approximately 500 W under normal operational conditions. The area not required for radiator use on the panels was insulated by multi layer insulation (MLI) blankets, as was the remainder of the spacecraft (S/C) body; continuity being broken only by the antennas (L-band and C-band, and vhf), ABM, launch adapter, AOCS sensors, and RCS thrusters.

A description of key characteristics within the TCS is presented in Fig. 2.

The notoriously thermally sensitive Ni-Cd batteries required special attention by the TCS in the form of: 1) conductive and radiative decoupling from the S/C, 2) baffled circular viewports to provide the required low-temperature level, 3) thermostatically switched heaters to maintain temperatures within the extremely tight operational limits (-5 to 15°C), and 4) a diffuser plate as an integral part of batteries to equalize internal gradients (required $\Delta T < 3$°C).

The ABM, situated within the satellite's central tube, was by necessity extensively decoupled from the S/C body, to

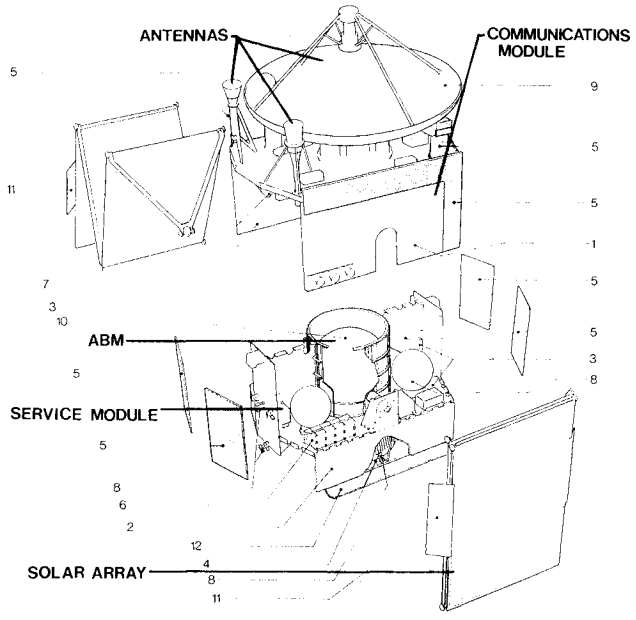

1. Payload radiators, partially covered with SSMs, Al-Kapton, Mylar insulation, locally thickened by thermal doublers, controlled radiation to S/C interior, TPA doubler with heat pipes.
2. Service module control radiator
3. Black paint on interior surfaces.
4. Kapton insulation with integrated VHF-shield.
5. Mylar insulation with integrated VHF-shield.
6. Battery thermal control (baffles, heaters)
7. Replacement heater for switched-off payload..
8. RCS Heaters
9. Antenna thermal control, white paint, insulation blankets on rear side and within antenna support bracket.
10. Kapton insulation around ABM
11. Fins on Solar Array
12. VHF-shield extension

Fig. 2 Key characteristics of the MCS-A thermal control subsystem.

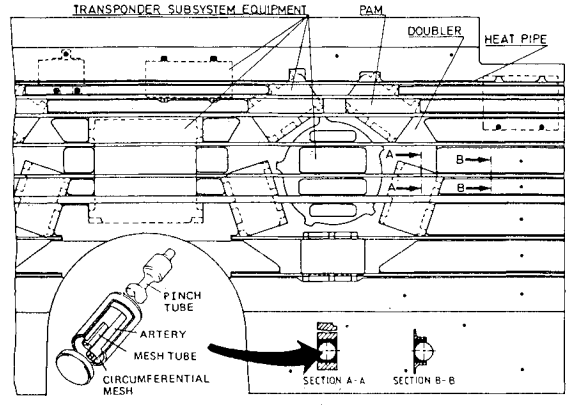

Fig. 3 TPA heat pipe radiator.

minimize heat soak back following motor firing and also to limit heat transfer during on-station operation. In addition to an MLI blanket envelope for the ABM body, MLI "patches" were fitted at the nozzle throat and exit (to be blown out at motor firing), and a ring of heaters installed on the lower dome of the ABM body. In this way, the ABM temperature could be maintained within limits (0-30°C) during the planned maximum of eight transfer orbits.

For active thermal control, four major categories of heaters were utilized for thermal control purposes:

1) Payload simulation heaters which compensate for TPA and/or TWTA operation in drift orbit as well as under non-nominal operating conditions to maintain a relatively stable dissipation in the C.M.

2) Three sets of heaters distributed strategically throughout the CM and SM so that, by selective ground control, the

north-south temperature gradients (during solstice) as well as the general temperature increase throughout the satellite from beginning to end-of-life conditions (material degradation) are minimized.

3) Thermostatically switched heaters used on the batteries, where exact thermal control is required due to the strict thermal requirements, and on the RCS flow control valves (FCVs) which are influenced by the severe external environment.

4) Ground controlled heaters used to regulate the ABM in transfer orbit. RCS line and tank heaters and payload substitution heaters required in certain configurations throughout the mission and switched on and off by ground command.

On MCS-A extensive use was made of MLI blankets. Two basic blanket packages were used: for a low-temperature environment (up to 120°C) a blanket core made up of 10 layers of aluminized Mylar was standard, and for areas exposed to temperatures > 120°C (satellite anti-Earth side during and after ABM firing), a blanket core made up of 18 layers of aluminized kapton was used.

Thermal verification of the MCS-A TCS was performed as shown in Fig. 4.

The major analytical tool was the overall satellite thermal mathematical model (TMM) of over 500 nodes which was used to analyze all of the critical mission phases, i.e., launch and ascent, transfer orbit, drift orbit sequence, and on-station critical phases. In addition, in-depth supportive analyses were performed on equipment/units requiring more detailed investigation, such as the TPA radiator, RCS thruster clusters, RCS hydrazine line network, battery, AOCS sensors, and ABM.

The solar simulation test (SST) performed with the protoflight S/C enabled direct verification of thermal control hardware and design, as well as providing a means of correlating the TMM. The final correlation results have been reproduced in Table 2.

Unfortunately, the satellite is not so well monitored in flight as in SST, with the TCS receiving telemetried data from only 54 sensors and not all of those are placed in thermally optimal positions. The nonoptimal positioning of certain sensors within dissipating units (PAM, battery, and vhf transponder) meant that the registered temperature was not always strictly equivalent to the mean unit temperature as produced by the TMM, thus SST provided an ideal opportunity for the "calibration" of the unit-associated sensors. An investigation into sensor /TMM nodal mismatch was also performed for the other sensors (not all sensors are optimally positioned at the nodal center, or directly on the border between nodes) and a set of correction factors (ΔT's) evolved to ensure a sound basis for comparison and to facilitate the illustration of future expected degradation in a statistically meaningful manner. A summary of these factors is contained in Table 3.

Table 2 Statistical comparison between test temperatures and analytical model predictions for MCS-A

Test	No. of sensors	Mean deviation (test-analysis), °C	Standard deviation, °C
T/O TP2	237	−0.46	3.52
T/O TP3	207	−0.40	3.00
O/S TP3	267	0.56	2.78
O/S TP5	260	−0.49	2.72
O/S TP6	260	−0.48	2.89
O/S TP4 (2)	263	−0.67	3.99

Flight Data

Transfer Orbit

The three major aspects affecting the thermal performance during the TO period are: launch pad environment, solar aspect angle (SAA), and number of transfer orbits (maximum of eight).

For the satellite, in general, the combination of nominal launch pad temperatures (22 ± 1°C), 88.7 deg SAA, and 3.5 TO duration resulted in temperatures near, but below, the predicted maximum. The only concerning aspect during this period was the high temperatures observed in both batteries. The high temperature was already obvious on the launch site where battery A was recorded at 26.7°C, this continued to rise until the higher than expected dissipation from the overcharged state of the batteries was reduced by a series of actions by ground control (during the first orbit). After reaching a peak of 32.6°C at Apogee 2, the battery temperature began to fall steadily until the end of the period. Selected temperature histories are presented in Fig. 5.

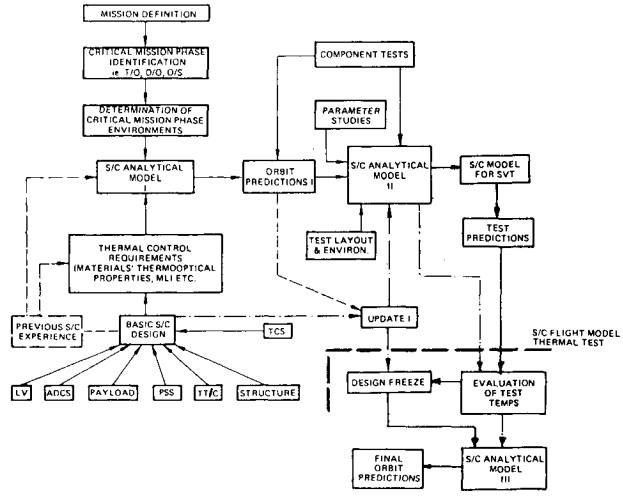

Fig. 4 Thermal verification plan for MCS-A.

Table 3 Correction factors applied to flight temperature sensors

Sensor position	Sensor ID	Correction factor[a]	Comment
ABM	1001	–	Not considered for evaluation, probably detached
SM lower floor	1002	+0.5	Node/sensor mismatch
SM shear wall	1009/10	+1.0	Node/sensor mismatch
SM radiator	1034	+10.0	Node/sensor mismatch
PAM (nonoperating)	1023-1033	−2.5	Position of thermistor
PAM (operating)	1023-1033	+6.5	within unit
vhf transponder – RX	T033,T028	+3.0	Position of thermistor
vhf transponder – TX	T028, T033	0	within unit

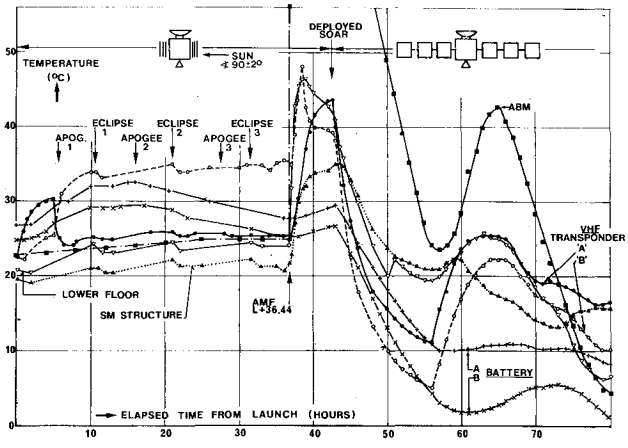

Fig. 5 Selected MCS-A post-launch temperatures.

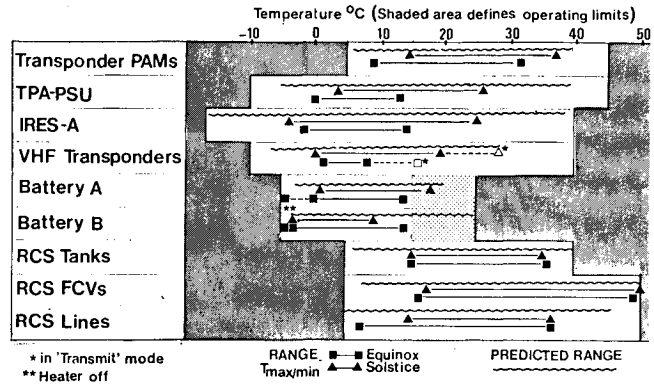

Fig. 6 Selected unit/component maximum flight temperatures.

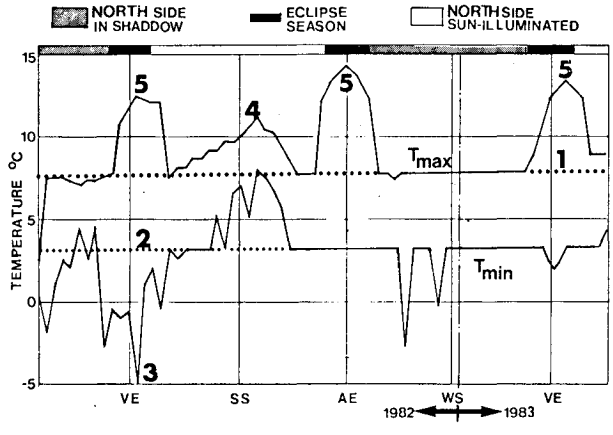

Fig. 7 Maxima and minima temperature history for Battery B: 1) heater automatic switch-off temperatures; 2) heater automatic switch-on temperature; 3) heater (HCU) switched off altogether; 4) summer solstice, warmest environment for battery; 5) maximum temperature at end of eclipse in all cases.

Drift Orbit

While there were no real thermal problems during this phase, it was evident that the soak-back effect was greater than predicted. Generally speaking, the temperature increases experienced in the satellite following apogee motor firing (AMF), although higher than expected (both vhf transponders and the batteries exceeding their prescribed limits for a short period), was not considered a problem. The cause of this is thought to lie in higher than anticipated ABM temperatures and/or larger than expected thermal coupling between ABM and the satellite body.

The remainder of this phase continued uneventfully for the TCS with the solar array being deployed 6 h after AMF, thus opening up the north and south radiator areas as well as unblocking the battery viewports. As the satellite rapidly cooled, the payload simulation and level heaters were switched on in a prearranged sequence over a period of about 6 h (see Fig. 5) to provide a nominal temperature level for the rest of this period.

On Station (O/S)

It can be stated that the general performance of the TCS during the first 18 months in orbit has been highly satisfactory, with all temperatures lying within the expected bandwidth. During this period dissipation within the satellite was higher than expected (~20 W at times) shifting the general satellite temperature level by up to +3°C in certain cases. The cause of this is attributed to two factors:

1) The transponder subsystem was configured in the 2+2 mode (4 PAMs) instead of the expected 3+3 mode (6 PAMs) since March, 1982, thus substitution heaters (providing more power than the difference in operating modes generate) were used to compensate.

2) Due to operational requirements, it was necessary to run the vhf transponder in the "transmit" mode with an increased dissipation of approximately 9W.

To counter the effects of these two factors the operational utilization of the level heaters was reviewed and it has been found that one of the general satellite level heaters can be switched off in compensation. This was carried out in March 1983 with almost immediate relief (3-5°C) for all units from the upper limits.

A general performance review of the thermally critical areas follows.

Unit/Equipment Temperature Limits

Collecting maximum and minimum unit/equipment telemetried temperatures throughout the initial 15 months while on-station and comparing them with their limits as in Fig. 6 shows that all temperatures lie within their prescribed limits. The predicted range of temperatures is also included for comparison.

TPA Heat-Pipe Doubler

PAM and ancilliary units have been maintained comfortably within limits. In order to assess the general performance of the heat pipes, it was first necessary to study the evolution of temperature gradients between the PAMs, and these are presented in Table 4 along with a comparable value from the SST. Between operating modules ΔT_{max} was <6°C (<10°C required) with no noticeable degradation over the annually comparable vernal equinoxes (VE) and summer solstices (SS), indicating continued flawless heat-pipe operation.

Battery Temperatures

Although remaining within predicted limits, the temperature of batter 1 at winter solstice (WS) was higher than anticipated (17.5°C) after one year. An exploratory thermal test was performed shortly after winter solstice during which it was observed that the temperature was reduced by 2°C by switching vhf transponder A (mounted near the battery) to B. This ΔT considered in addition to the warmer than anticipated general temperature levels results in a "corrected" battery temperature very near that nominally predicted. The complete temperature history for battery B since launch is presented in Fig. 7 from which the various seasonal phases can be identified as well as the functioning of the automatically controlled heaters (switching "on" at 2.5°C and "off" at 7.5°C, approximately).

Table 4 Temperature gradients between operating PAM's

Date	TPA[b] configuration	Instantaneous ΔT between operating PAM's	
		Maximum over 24 h	Minimum over 24 h
MCS-B SST TP-4[a]	3+3	2.4	–
Jan. 24, 1982	3+3	2.8	2.3
VE 82 March 20, 1982	2+2	5.6	3.9
SS 82 June 30, 1982	2+2	4.7	3.4
AE 82 Sept. 26, 1982	2+2	5.3	4.7
WS 82 Dec. 23, 1982	2+2	4.8	4.2
Jan. 24, 1983	2+2	4.7	4.7
VE 83 March 23, 1983	2+2	5.1	4.8
SS 83 June 22, 1983	2+2	4.1	2.4

[a]Roughly equivalent case to Jan. 24, 1982, solar beam in test 23.5 deg (−19 deg for Jan. 24, 1982). [b]Number of operating PAM's (two or three from each cluster of five may be on). All 2+2 configurations shown use the same modules in each case.

Table 5 Periods selected for thermal investigation and quality of 24-h cyclic reproduction

Date	Sensor reading ≤1 bit[a] difference, %	Payload[b] configuration	Comments
Jan. 25, 1982	94	3+3	Last day of thermal calibration test. Payload operating in ATP.
March 20, 1982	94	2+2	Vernal equinox 1982. Payload operating in ATP (day of maximum eclipse).
June 30, 1982	85	2+2	Nearest date to summer solstice 1982 with relatively stable data. Payload operating.
Sept. 26, 1982	93	2+2	Autumnal equinox 1982. Payload operating (near maximum eclipse).
Dec. 23, 1982	85	2+2	Winter solstice 1982. Payload operating.
Jan. 24, 1983	89	2+2	Enabling calculations to determine annual degradation rates. Payload operating.
March 23, 1983	81	2+2	Vernal equinox 1983. Lower level of reproducibility caused by automatic heater switching (unsymmetric effect over 24 h).
June 22, 1983	93	2+2	Summer solstice

[a]One data bit: for temperature sensors, one bit variation is between 0.2 and 2.5°C or approximately 0.6% of the range. [b]Operating mode of transponder subsystem.

RCS Temperatures

Without exception all hydrazine associated equipment have been maintained well above the critical 9°C lower limit ($\Delta T > 9$°C), and for most components a sufficient margin exists from the upper limit although the general satellite temperature level was warmer than expected. Within one thruster pair, however, FCV temperatures peaked near the upper limit (50°C). The reason behind this unexpected T_{max} has been identified and it is not anticipated to present any problems, with subsequent relief achieved following the reduction of internal satellite heater power.

General Thermal Control Aspects

Only one incident of a failure affecting TCS equipment has been observed—that of the battery prime heater circuit, which was replaced by the redundant system in August 1982 following observed eccentricities in battery temperatures. Subsequent testing has isolated the failure in one of the circuits within the heater control unit (HCU).

Thermal Effects of Material Degradation

Degradation mainly affects the reflectivity of surfaces in the solar spectrum and generally leads to a reduction in this property. Changes in the infrared spectral region are, with few exceptions, of comparatively minor importance. Thus degradation results in additional absorbed heat in the satellite and consequently in a gradual temperature rise during the mission life.

Unlike its predecessor, OTS-2, MCS-A is a commercial satellite, thus the satellite configuration at the thermally interesting periods (solstices, equinoxes) could not be controlled by the TCS, however, after many years of experience in the utilization of OTS-2 in-flight thermal data,[4] it was confidently expected that the relatively limited amount of MCS-A data could be processed to provide pointers on degradation rates. Periods of thermal stability (ΔT over 24 h small or negligible) were selected near or at winter and summer solstices, vernal and autumnal equinoxes (periods of maximum eclipse duration), and the thermal calibration test. The actual dates and quality of thermal data are presented in Table 5, satellite configurational data and heater status for the same periods are presented in Table 6.

To assess the effects of degradation, threefold use can be made of the MCS-A flight data for these periods.

1) Collective Sensor Comparison. The most simple and unambiguous method of determining any degradation effects on a spacecraft is a direct comparison of temperatures at

Table 6 Satellite operating configurations and dissipation for selected periods

	Average dissipation over 24 h,[a] W							
	Jan 82	VE 82 (sunlight)	SS 82	AE 82	WS 82 (sunlight)	Jan 83	VE 83 (sunlight)	SS 83
Overall spacecraft[b] dissipation	572	611	585	668	569	570	620	559
Payload	355	282	282	282	282	282	282	282
RF output	66	43	43	43	43	43	43	43
TTC	32	32	32	32	32	32	32	32
PsS[b]	26	26	26	26	26	26	26	26
AOCS	46	46	46	46	46	46	46	46
TCS								
RCS and battery heaters	19	21	17	17	16	16	18	17
Level heaters	301	130	50	130	31	31	81	50
Sub heaters	0	31	92	92	92	92	92	61
Total	575	611	588	668	568	568	620	557
PSS								
SRU	48	46	39	45	46	46	45	39
Battery charge	14	14	14	14	14	14	14	14

[a]See Table 6 for exact date. [b]From onboard sensors (main bus voltage times current), average over one daily sunlit period. [c]Excluding SRU and battery charging circuits (separate from main bus).

Table 7 Effects of degradation derived by the collective sensor comparison

	Observed[a] ΔT, C	Observed ΔQ, W			Equivalent[c] ΔT, °C			Equivalent degradation effect, °C
Annual period	(A)	Internal[b]	Radiators[c]	Others[d]	Internal (B)	Radiators (C)	Others (D)	A − (B + C + D)
Jan. 83-Jan. 82	3.60	−1.5	19.7	−3.6	−0.17	1.16	−0.14	2.75
VE 83-VE 82	0.16	−49.5	61.1	−1.2	−5.5	3.59	−0.04	2.11
SS 83-SS 82	1.51	0.0	−26.3[f]	0.0	0.0	−1.55	0.0	3.06

[a]Mean annual difference of T_{max} taken from internal sensors unaffected by configuration/heater changes.
[b]General level heaters and/or RCS line and tank heater changes.
[c]Payload configuration and/or substitution heater changes.
[d]SRU and/or FCV heater changes.
[e]Sensitivity, 9, 17 and 30 W/°C for internal, radiators, and others, respectively.
[f]−30.7 W for heaters, +4.4 W for varying SAA (June 30, 1982, June 22, 1983).

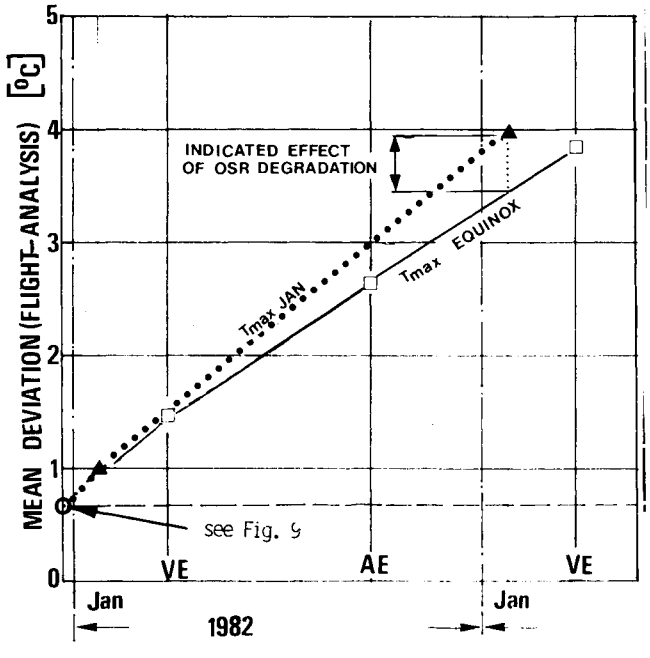

Fig. 8 Orbital mean temperature increases determined by TMM.

exactly the same operating conditions. Due to the varying satellite configuration at comparable periods, a method was evolved by which the observed ΔTs could be compensated by correction factors based on the satellite response to variations in dissipation, i.e., 1°C per 9.0 W of internal dissipation and 1°C per 17 W of radiator dissipation.

From the available data, annual comparisons could be made between vernal equinoxes and summer solstices (1982 and 1983) as well as the annual difference for the calibration test. A summary of results is presented in Table 7. The data from autumnal equinox (AE) was not used in this comparison since it can be seen from Table 7, that the difference in power level within the satellite is relatively high in comparison to the other equinoxes (>50 W). It is considered that this figure induces unacceptable uncertainties to this form of comparison and, therefore, is excluded.

The associated uncertainties with this means of comparison require that the results can only be considered as approximate; however, it does shown an unexpectedly large annual increase at equinox. The difference between the equinox and January degradation values may (as a rough approximation) be attributed solely to the effect of the north radiator OSRs, indicating a $\Delta\alpha_s$ of 0.023, according to the sensitivity of the satellite ($\Delta T = 1$°C per $\Delta\alpha_s$ of 0.035).

2) Computer-Aided Comparison using TMM. By performing thermal analysis for the exact operational condition of the

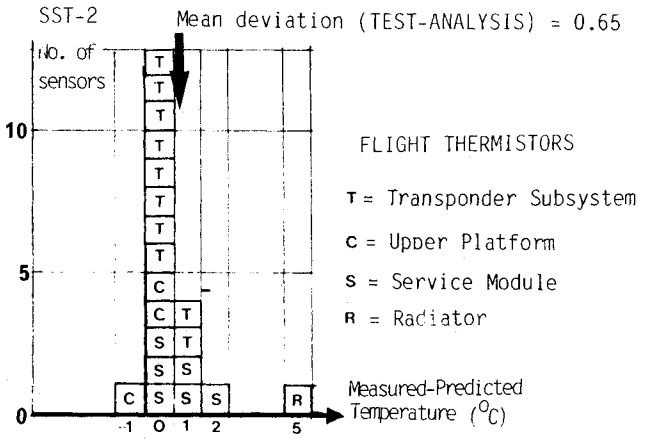

Fig. 9 Correlation of TMM with flight sensor readings during ground test.

satellite, the difference between predicted and actual temperatures can be obtained, and by maintaining beginning of life (BOL) thermal-optical material properties within the TMM, the effects of degradation can be observed on an annual (biannual for equinox) basis. The results are presented graphically in Fig. 8 and confirm the trend observed by method 1 above. To obtain a start point for this curve, the correlation of the TMM with flight sensors taken from ground test was used. This was derived as shown in Fig. 9.

The differences between flight and predicted temperatures for equinoxes and January are presented in Fig. 8 which, for the sake of comparison, have been graphically connected linearly. It is too early as yet to begin postulating on future trends, however, two major aspects emerge from Fig. 8.

1) There is a significant general rate of temperature increase identified by observing the results from equinox seasons (at an initial rate almost identical to that observed on OTS-2).

2) The additional rate of temperature increase attributable to north/south (OSR) degradation ($\Delta T \sim 0.6°C \Rightarrow \Delta\alpha_s \sim 0.21$) is within the expected range and a vast improvement over OTS-2.

One aspect to emerge from this comparison is the difference in predicted diurnal variations from those observed in flight. The latter values appear in every case to be larger in comparison, especially on the radiator sensors, and may be wholly or partly attributable to the following factors:

a) The variable view factor from the radiators to the solar array was averaged over 24 h for the TMM, in practice this can vary between 2-8% locally.

b) Temperature variation between front and rear sides of the solar array (SOAR).

c) The shadow of the yoke as it traverses 360 deg on the radiator causes local temperature troughs, not picked up by the TMM.

d) vhf shield and antenna shadows.

e) Unknown direction qualities of OSR optical properties.

f) Overestimation of thermal capacity or local disturbance by temperature sensor.

3) Individual Assessment of Degradation Effects. Although no specific degradation experiment was flown on MCS-A, it is possible, by correct selection of certain individual sensor temperatures and analytical methods, to obtain an approximation to values of annual degradation associated to specific materials onboard.

Candidate areas for study and associated materials are shown in Table 8, from where it can be deduced that only with the TPA-PSU radiator does the data exist to evaluate the annual degradation of the sun-illuminated materials. The method by which this is performed is similar in each case and involves the contrived iterative process as described in Fig. 10.

This contrived analysis method is necessary since the lack of sufficient sensors available to define the local environment

Table 8 Areas selected for study of individual degradation effects

Sensor	Position in satellite	Sun-illuminated	Material
TPA PSU doubler	South radiator (CM)	Sept.-March	OSR
TPA PAM	North radiator (CM)	March-Sept.	OSR
SM radiator	North radiator	March-Sept.	OSR
Galileo ir sensor	Upper floor (CM)	March-Sept.	Aluminized Teflon radiator

means that absolute indicated flight temperatures cannot be realistically used, however, the difference over annual periods is regarded as meaningful.

For comparison purposes, the sensor positioned on the TPA-PSU the annual degradation for the period January 1982 to January 1983 was evaluated and plotted in Fig. 11 along with the curve of OSR degradation calculated for OTS-2. The analysis method was checked for the nonsolar-illuminated periods (AE 82, VE 82, and VE 83) and a very good predictability of the radiator temperature was achieved ($\pm 0.3°C$, which is on the same order of magnitude as the telemetried bit).

Interpretation of Results

A synthesis of the results from the three methods support a number of conclusions:

1) There is a noticeable general temperature increase in the satellite.

2) Degradation is noticeable during equinox conditions (at a rate greater than expected).

3) There is additional degradation (at the expected rate) where the radiator is solar-illuminated.

4) The initial degradation rates do not appear to be as large as those observed on OTS-2.

It is, perhaps, too early to make definitive statements on how the satellite will behave for the remaining six years of its mission, however, the initial impression is that apart from certain minor deviations, the MCS-A thermal performance appears to be nominal.

The major impact of material degradation in equinox will come from the MLI outer surface and antenna. By assuming worst-case values for the expected degradation over one year—L-band antenna (white paint), $\Delta\alpha_s = 0.025$ and Kapton (MLI outer layer), $\Delta\alpha_s = 0.07$—and using calculated values for satellite sensitivity to these changes, only about 50% of the indicated degradation in equinox can be accounted for. Any conclusions from this data, however, must be made in a tentative manner until substantiated trends from autumnal equinox and biennial comaprisons can be identified.

A similar occurrence, although to a slightly greater degree, occurred in OTS-2, which has still not been fully explained and which is presently being investigated. Possible causes have been opinioned, which include:

1) Stronger MLI outer layer degradation than expected, either from contamination (AMF, thruster plumes) or simply underestimation of spatial environment effects.

2) Delamination or dealuminization of MLI resulting from such a method as electrostatic discharge (ESD). MCS-A has indeed experienced several ESDs; in fact, in February 1982, a severe ESD had major repercussions throughout the satellite and may have damaged thermal control materials. The paucity of sensors in the region of areas likely to be affected means that this will be determined only by observation of long-term temperature trends within the satellite.

3) Stronger degradation of apendages (adapter, thrusters, antennas, AOCS sensors). The available sensors indicate that this could occur only on the adapter and antennas; the effect, however, is not likely to be large.

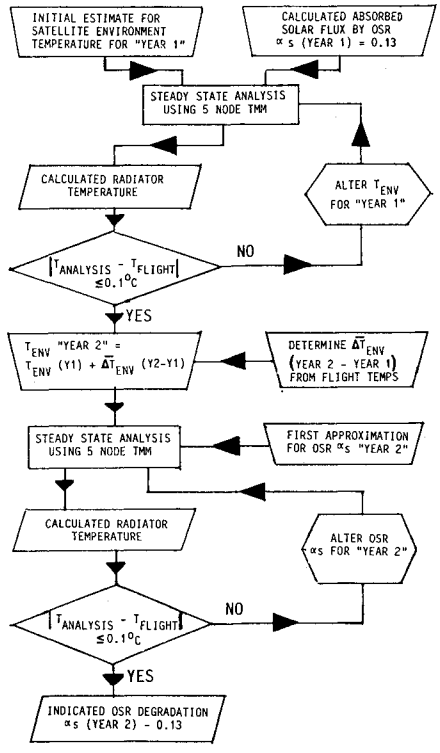

Fig. 10 Flow diagram of iterative process used for the assessment of individual degradation effects.

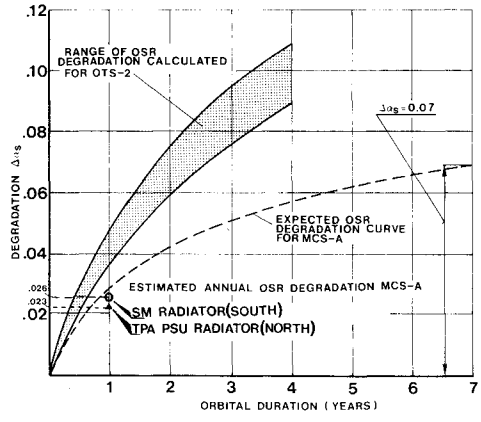

Fig. 11 Comparison of calculated and expected degradation effects on MCS-A as well as on OTS-2.

Therefore, it must be stated that the degradation sources effective in equinox are not completely explained and probably will remain so until more in flight data become available, and a pattern or trend has been extracted.

From the January comparison, the only additional factor introduced from the equinox comparison is the effect of degradation of the radiator OSR, which can be roughly allocated to the observed difference. Within the tolerances of the methods, the amount of OSR degradation is in reasonable agreement between 0.02-0.03 ($\Delta\alpha_s$) over the initial annual period, which compares favorably with the predicted degradation curve.

Conclusions and Future Trends

In comparison with OTS-2[4] the initial degradation rates do not seem to be so severe and more in line to that expected. This also adds further support to the opinion that the OSR degradation observed on OTS-2 was partly or even mostly attributable to contamination, especially from the plume during AMF. On MCS-A the gaps between solar array and radiators are partially closed during AMF by the vhf shield extension and fins, unlike OTS-2 which was open.

MCS-A is the first satellite of the ECS-type family from which more than nine derivatives are expected to be launched within the next five years. Therefore, it is important that the in-flight information from MCS-A as well as its predecessor, OTS-2, be fed back into the various programs. The observable trends and recommended action performed thus far include:

1) Higher than expected OSR degradation observed on OTS-2[5] led to an increase in the analytical value for degraded OSR α_s values ($\Delta\alpha_s = 0.07$ instead of earlier 0.03 for seven years) on MCS and ECS, as well as being the major reason for flying a dedicated degradation experiment on ECS-F1.

2) High battery temperature on OTS-2 and MCS-A during TO and O/S has led to improvements to the actual thermal design of ECS-F2, coupled with a revised charging process from the PSS, which together will ensure that the battery temperatures should no longer be a problem on future launches. On MCS-B,† launch pad charge management by the PSS resulted in average battery temperature of >20°C, an improvement of over 7°C on MCS-A.

3) The observed higher than expected heat soak-back effect following AMF on OTS-2, MCS-A, and Intelsat V (Ref. 6) (in each case by approximately 50%) indicates that the thermal performance of the satellite is still not fully understood during this period and has resulted in an extra temperature sensor (with high-temperature measurement capability) being fitted to the ECS-F1 ABM, in an attempt to obtain real ABM temperature data during an in-flight AMF. The information provided by this sensor has indicated[7] that the actual ABM temperature post-AMF may, in fact, be underestimated.

4) The observed higher than expected diurnal variatons of certain sensors on OTS-2 and MCS-A has led to a review of possible causes as described in the previous section (Interpretation of Results).

The present nominal performance of the MCS-A TCS is encouraging, it shows that the employed thermal design philosophy was correct and that future satellites belonging to the ECS family can be launched with assurance that the onboard equipment will be provided with a benign thermal environment.

Acknowledgments

The author wishes to acknowledge the invaluable support provided by K. Derbyshire of ESA as well as colleagues within the Thermal Control Department at ERNO for many helpful discussions. Thanks also to Janet Haigh for typing and retyping this manuscript.

References

[1]McLaurin, D.E., and Gregory, D.N., "General Description of the Orbital Test Satellite," Paper No. IEE CP 199, IEE/IOP Conference, London, April 1981.

[2]Stümpel, D., "OTS Thermal Design and In-Orbit Performance," ESA Symposium SP 139, 1978.

[3]Chalmers, D.R. and Stümpel, D., "MCS-A Thermal Control Subsystem," SAE Paper 820862, 1982.

[4]Chalmers, D.R., "In-Orbit Degradation of Thermo-optical Material Properties on OTS-2," SAE Paper 820863, 1982.

[5]Bouchez, J.P., and Gülpen, J., "The European Geostationary Communications Satellite OTS—Two Years of Thermal Control Experience in Orbit," AIAA Paper 80-1500, 1980.

[6]Spencer, A.L., et al., "Intelsat V Thermal Design, Testing and Flight Performance," AIAA Paper 82-0863, 1982.

[7]Chalmers, D.R., "ECS-1 Thermal Control Flight Performance Assessment," ERNO AN RT551-127/83.

†The second MCS satellite did not become operational due to launcher failure.